J Mater Sci (2018) 53:8302–8313

Computation

Structure, bonding, stability, electronic, thermodynamic and thermoelectric properties of six different phases of indium nitride

Vipin Kumar[1] and Debesh R. Roy[1,*]

[1] *Department of Applied Physics, S.V. National Institute of Technology, Surat 395007, India*

Received: 18 August 2017
Accepted: 24 February 2018
Published online: 6 March 2018

ABSTRACT

Density functional investigation is carried out on the structure and bonding, stability, electronic, thermodynamic and thermoelectric properties on the six different phases of indium nitride. In addition to the monolayer hexagonal, zinc blende, wurtzite and rock salt, two more new possible phases, viz. caesium chloride and nickel arsenide, are also explored. The calculated crystal parameters for all six phases are compared with available experimental and theoretical values. Band structure and density of states are predicted for understanding their behaviour in metal–insulator–semiconductor domains as well as the contribution of their different atomic orbitals around the valence and conduction band edges. Phonon dispersion curves are generated to understand the dynamical stability of the considered indium nitride phases. Further, a detail comparative study is performed on various thermodynamic and thermoelectric properties of the dynamically stable indium nitride phases. An electron density contour is also generated for the stable phases to understand the nature bonding between indium and nitride in those phases.

Introduction

Indium nitride has gained a significant amount of attention in recent days for its various promising applications in different fields [1–7]. Compared to other group III-nitrides, InN is noticed to be in primary focus of the researchers due to its narrow band gap, smallest effective mass, highest electron mobility and almost invariant band gap on temperature. Efforts have been tendered to explore the possible applications of InN including field effect transistors, lasers, solar cells, photodetectors and thermoelectrics [1–7]. In general, group III-nitrides have been viewed as a promising framework for semiconductor gadgets applications, particularly for the improvement in blue and ultraviolet LED's [1–9]. It is reported that aluminium nitride (AlN), gallium nitride (GaN) and indium nitride (InN) does posses comparative potential towards opto-electrical applications in appropriate photon energies [8]. The other III-nitrides group, e.g. thallium nitride (TlN), is also investigated with its different phases which show their narrow

Address correspondence to E-mail: drr@phy.svnit.ac.in

https://doi.org/10.1007/s10853-018-2176-9

band gap and mostly semi-metallic behaviour [9]. From the experimental side, cubic zinc blende phase of InN (*zb*-InN) as well as [10, 11] the wurtzite phase (*w*-InN) [12, 13] have been synthesized. At higher pressure, rock salt phase of indium nitride (*rs*-InN) is also observed [11]. In a recent work [14], theoretical investigation under density functional theory is performed on the possible hexagonal monolayer phase of InN (*h*-InN). However, most of the studies exclusively have been done on *w*-InN, due to its high stability and narrow band gap (0.6-0.7 eV) [15]. Few studies are also focused on the *zb*-InN phase [16–18]. However, although the compound possesses a huge future possibility, very little work is attempted on the investigation of other possible phases, like rock salt and/or single layer. And, none of the comparative studies has been performed to report on the various physicochemical properties, e.g. structure, bonding, electronic, vibrational, thermodynamic and thermoelectric properties of the various possible phases of indium nitride.

The purpose of the present work is to report a detailed investigation for the first time on the various physicochemical properties of six different phases of indium nitride, viz., monolayer hexagonal (*h*-InN), zinc blende (*zb*-InN), wurtzite (*w*-InN) and rock salt (*rs*-InN) along with the search for two new possible phases: caesium chloride (*cc*-InN) and nickel arsenide (*na*-InN), under density functional theory [19, 20]. The optimized structural parameters for all the six phases are reported and compared with available experimental and other theoretical results. Electronic band structures along with total and partial density of states are predicted to understand the metal–insulator–semiconductor (MIS) nature of the material at different phases. To understand the dynamical stability of all the considered phases, phonon dispersion curves (PDC) are calculated which are not available experimentally. Further, various thermodynamic properties, viz. specific heat (C_v), entropy (S), internal energy (U) and Helmholtz free energy (F), are calculated and compared first time for the dynamically stable phases of InN. The electrical (σ) and thermal (κ) conductivities are calculated and compared for the first time for dynamically stable phases of InN to understand their usefulness in thermoelectric applications. To understand the nature of bonding in the stable phases, we have also predicted and explained electron charge density maps.

Computational details

First principles calculations based on fully self-consistent density functional theory (DFT) [19, 20] with the Kohn–Sham approach [20] has been used to calculate the fundamental eigenvalues. A very popular and reliable generalized gradient approximation (GGA) exchange–correlation potential, viz. Perdew–Burke–Ernzerhof (PBE) [21], has been utilized for all calculations. The actual calculations were carried out using the QUANTUM ESPRESSO code [22] which uses self-consistent field approach using plane-wave basis set to compute total energies. Also, our calculations includes the norm conserving pseudo-potential for In and N atoms with scalar-relativistic effects. For the monolayer hexagonal phase of InN, a vacuum of 15 Å is considered for interaction between two adjacent planes introduced by Born-von Karman periodic conditions [23] in the super cell approach employed during the construction of monolayers. Electron wave functions were expanded in the plane-wave basis sets. The kinetic energy cutoff used for the plane-wave basis sets are as 45 Ry, 50 Ry, 60 Ry, 60 Ry, 55 Ry and 55 Ry for hexagonal monolayer, wurtzite, zinc blended, rock salt, caesium chloride and nickel arsenide phases, respectively. Monkhorst–Pack *k*-point sampling is used as 11 × 11 × 1 for the hexagonal monolayer and 15 × 15 × 15 for the other five phases of InN. For the convergence of the total energy, we have used 10^{-10} Ry in the self-consistent field calculation. The forces on each atom are converged below 0.01 eV $Å^{-1}$ during the structural optimization of both unit cell dimensions and atomic internal coordinates. All geometrical structures were plotted using XCrySDen software [24]. To investigate the dynamical stability of the considered phases of InN, we have calculated their phonon spectra as well as cohesive energies using density functional perturbation theory (DFPT) [25]. Various thermodynamic functions, viz. constant volume specific heat (C_v), entropy (S), internal energy (ΔU) and vibrational part of Helmholtz free energy (ΔF), are calculated using the quasi-harmonic approximation (QHA) [26] under DFPT.

The thermoelectric transport properties, viz. electrical and thermal conductivities, are predicted utilizing BoltzTraP code [27] with constant scattering time approximation (CSTA) [23] and rigid band approximation (RBA) [28, 29]. As per the RBA, the band structure doesn't change with the shifting of

Fermi level, i.e. shifting of the Fermi level only results for the variation of electron and hole concentrations as the donor and acceptor doping levels are varied. In CSTA approximation, the scattering time of an electron is assumed to be independent of energy of the electron, but depends on doping and temperature. The transport properties, viz. electrical conductivity (σ) and electronic thermal conductivity (κ^e), are calculated using Boltzmann semiclassical equations as follows:

$$\sigma_{\alpha\beta}(T;\mu) = \frac{1}{\Omega}\int \sigma_{\alpha\beta}(\varepsilon)\left[-\frac{\partial f_\mu(T;\varepsilon)}{\partial_\varepsilon}\right]\mathrm{d}\varepsilon \quad (1)$$

$$\kappa^0_{\alpha\beta}(T;\mu) = \frac{1}{e^2T\Omega}\int \sigma_{\alpha\beta}(\varepsilon)(\varepsilon-\mu)^2[-\frac{\partial f_\mu(T;\varepsilon)}{\partial_\varepsilon}]d\varepsilon \quad (2)$$

where k^0, T, e, α and β, Ω, f_μ and μ are the electronic part of thermal conductivity, absolute temperature, electronic charge, tensor indices, volume of unit cell, Fermi–Dirac distribution function and chemical potential, respectively. The electrical conductivity (σ) is expressed in terms of the ratio of σ/τ, where τ is the relaxation time.

Result and discussion

Structural and electronic properties

In order to investigate various electronic, thermodynamic, thermoelectric properties as well as dynamic stability and nature of bonding in various indium nitride phases, we have optimized their crystal structure and lattice parameters. Figure 1 shows the optimization of the lattice constant to achieve its equilibrium value that corresponds to the minimum total energy along with the unit cells architecture of various indium nitride phases. The fully relaxed lattice parameters for various indium nitride phases are achieved as 3.54 Å (*h*-InN), 3.58 Å (*w*-InN), 5.05 Å (*zb*-InN), 4.71 Å (*rs*-InN), 2.99 Å (*cc*-InN) and 3.45 Å (*na*-InN).

Table 1 represents the space groups, calculated lattice parameter (a, c) along with available experimental and other theoretical data [30–39], and cohesive energy (E_c) of various indium nitride phases. It may be noted that the predicted lattice parameters are in well agreement with available experimental and other theoretical results. In order to find the strength of binding among the atoms in all the InN phases, we have computed the cohesive energy which is defined as the difference between the total electronic energy of a solid and its constituent neutral atoms as follows:

$$E_c = E_{(\mathrm{InN})} - \left[E_{(\mathrm{In})} + E_{(\mathrm{N})}\right] \quad (3)$$

where $E_{(\mathrm{InN})}$ is the total energy of the system, and $E_{(\mathrm{In})}$ and $E_{(\mathrm{N})}$ are the total energy of indium and nitrogen atoms, respectively. It may be noted that the wurtzite phase shows maximum stability (E_c = 15.91 eV) compared to others. The *na*-InN phase (chosen to be a new phase) also shows large cohesive energy (9.75 eV). The *h*-InN (7.19 eV) and *zb*-InN (7.13 eV) also shows significant inter-atomic bonding strength. Caesium chloride phase shows the least binding stability (4.04 eV) among the all considered InN phases.

Figure 2 shows the self-consistent scalar relativistic electronic band structure of various indium nitride phases. The monolayer shows an indirect band gap of 0.43 eV (Γ–K point) and a direct gap of 0.88 eV (Γ point), showing a semiconductor in nature. The PBE-GGA estimation of band gaps for the *w*-InN and *zb*-InN shows a very small positive value close to zero gap as expected due to the well-known shortcoming of underestimation of energy band gap in many of the DFT-GGA methods [40]. Such underestimation arises due to the simple forms of exchange correlation which are not sufficiently flexible to reproduce both the exchange correlation energy and its derivative. In recent past, Borges and Scolfaro [41] have shown that a modified Becke–Johnson exchange potential (mBJ) [42] can make a better estimation of the band gap as 0.65 eV with experimental results (0.6-0.7 eV) [43, 44]. A close to zero band gap (very small negative value) for *rs*-InN (− 0.06 eV) and *na*-InN (− 0.13 eV) phases are found at the Γ point, whereas caesium chloride (*cc*-InN) phase came out to be metallic in nature. The qualitative energy band gaps as well as the larger cohesive energies of *h*-InN and *na*-InN phases identify them as potential candidates for future investigation at different ambient conditions. It may be noted from a recent report [45] that the GGA-PBE method may underestimate band gap value due to its lack of derivative discontinuity in KS potential, an advanced functional like SCAN meta-GGA, HSE06 may be useful. Since the main focus of the present study is to carry out a detail comparative study on various phases of InN to identify their individual efficacy for specific potential applications, where high quantitative accuracy was not the priority, we didn't

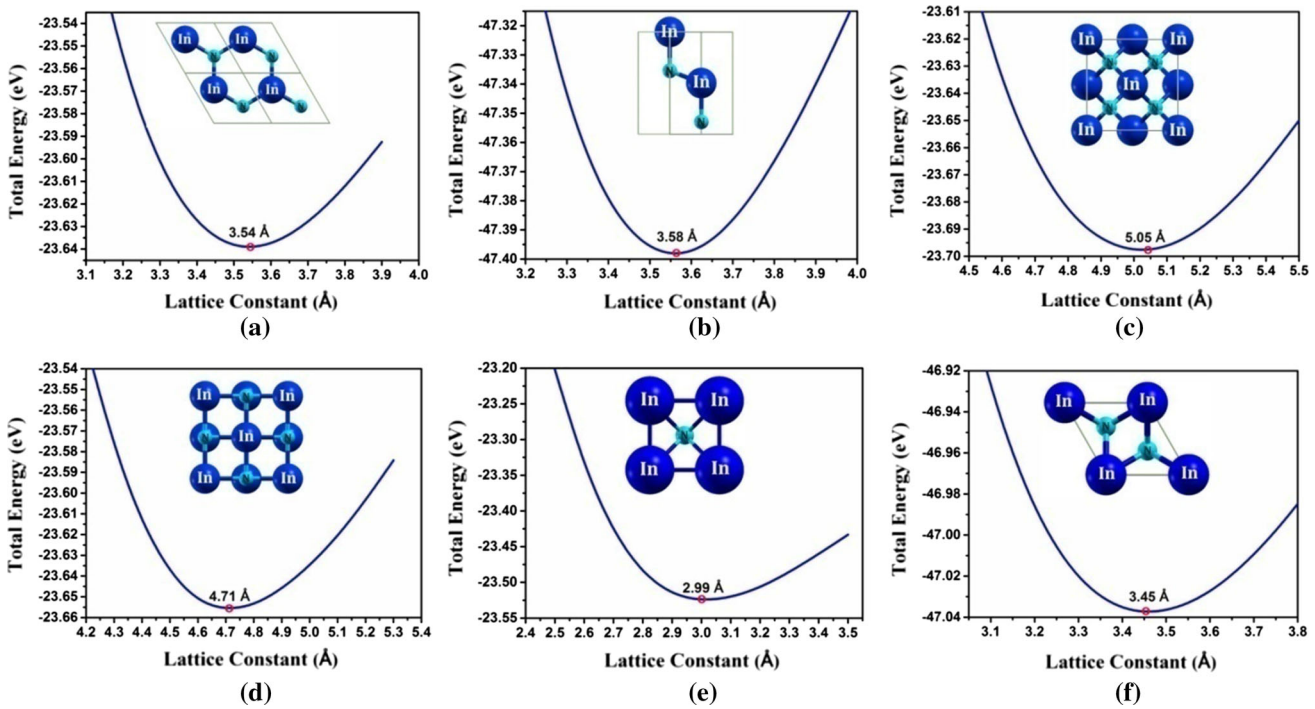

Figure 1 Total energy versus lattice constant for finding equilibrium lattice parameter for **a** monolayer hexagonal, **b** wurtzite, **c** zinc blende, **d** rock salt, **e** caesium chloride and **f** nickel arsenide phases of indium nitride. The crystal structures are represented in inset.

Table 1 Space groups (SG), calculated lattice parameter (*a*, *c*) with available experimental and other theoretical data and cohesive energy (E_c) of various indium nitride phases

No.	Structure	SG	*a*/*c* (Å)	Other calc. (Å)	Expt. (Å)	E_c (eV)
1	*h*-InN	P6/mmm no. 191	$a = 3.62$; $c = 18$	3.63 [14]	–	7.19
2	*w*-InN	P63 mc no. 186	$a = 3.58$; $c = 5.79$	3.54 [30], 3.63 [31], 3.60 [32]	3.53 [33], 3.54 [35]	15.91
3	*zb*-InN	F-43 m no. 216	$a = 5.05$	4.97 [33], 4.98 [34]	–	7.13
4	*rs*-InN	Fm3 m no. 225	$a = 4.71$	4.61 [31], 4.62 [33], 4.70 [37, 38]	4.53 [36] 4.65 [39]	6.11
5	*cc*-InN	Pm3m, no. 221	$a = 2.999$	–	–	4.04
6	*na*-InN	P63/mmc no. 194	$a = 3.33$; $c = 4.60$	–	–	9.75

attempted such level of calculations in the present work.

In order to understand the contribution of various atomic orbitals to the valence and conduction energy bands, we have computed the total (TDOS) and atomic site-projected density of states (PDOS) for all the considered indium nitride phases. The TDOS and PDOS of various InN phases are represented in Fig. 3.The total DOS describes the number of states per interval of energy at each energy level that are available to be occupied or investigate the nature of the states forming the valence and conduction band edges, and partial DOS distinguish the contribution of the individual atomic shells to the band edges. Moreover, to understand the electronic properties we make projected density of states (PDOS) in Fig. 2. It may be noted that the valence band edge of *h*-InN (Fig. 2a) is mostly composed of the N-2*p* states with some contributions from In-5*p* states, while the conduction band edge is made of mostly by the In-5*p* states. For *w*-InN (Fig. 2b) and *zb*-InN (Fig. 2c) phases, the valence band edge is mainly composed of *p*-contribution from both the N and In atoms, whereas the conduction band edge is composed of 2*s* and 2*p* states of nitrogen and 5*s* states of indium. Again, for *rs*-InN phase, *p*-orbitals of N and In

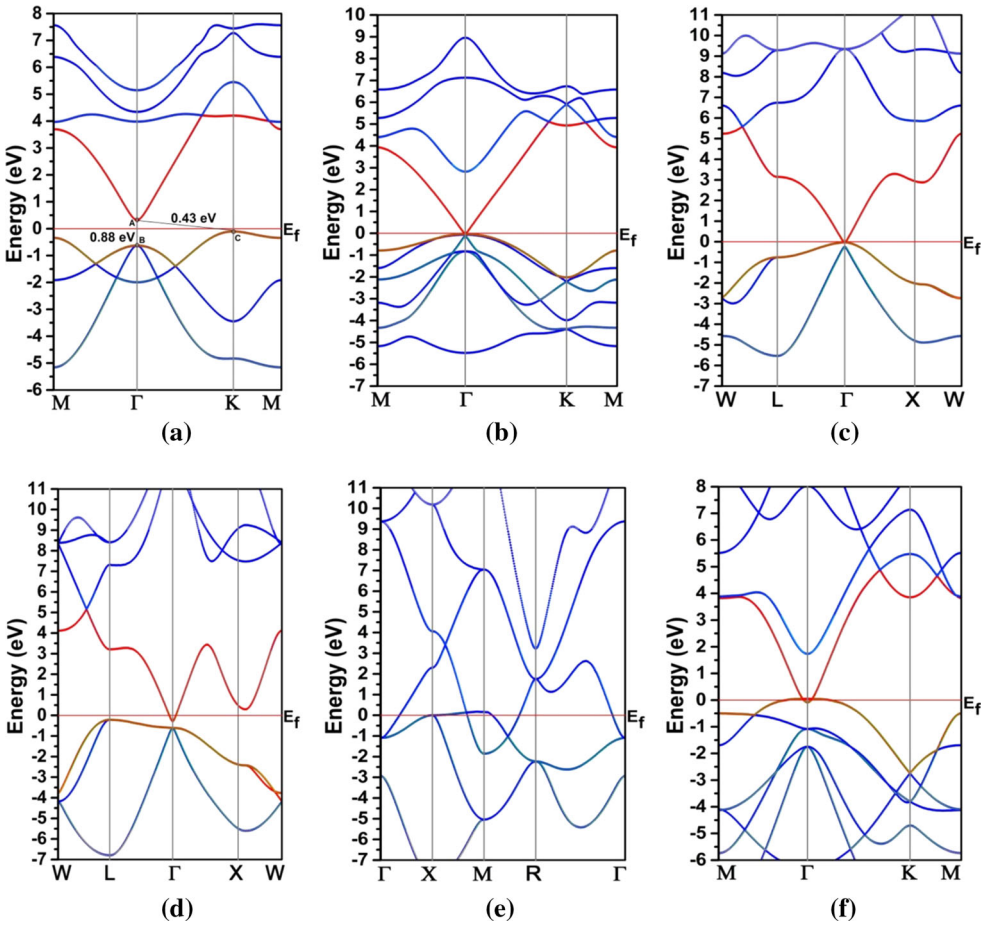

Figure 2 Electronic band structures of **a** monolayer hexagonal, **b** wurtzite, **c** zinc blende, **d** rock salt, **e** caesium chloride and **f** nickel arsenide phases of indium nitride.

dominates at the valence edge compared to others, resulting a small band cross at the Fermi level. In both the *cc*-InN and *na*-InN phases, both the conduction band minimum (CBM) and valence band maximum (CBM) crossing the Fermi level with a dominating contribution of the p-states of nitrogen and indium atoms. Overall, it may be noted that for all the six indium nitride phases, p-states of nitrogen dominates in the valence band edge, and also mostly contributes in the conduction band edges. The *p*-orbital of In also contribute with a notable amount in both the valence and conduction band edges. The domination of the N-2*p* states at the Fermi level may be understood as the more electronegativity of the nitrogen (3.04 eV) compared to indium (1.74 eV) as per the Pauling theory [46], which results an attraction of electrons from In by the nitrogen atom. In all the six phases, it is noticed that the contribution of 4*d*-states of indium near the top of the valence band as well as bottom of the conduction band is very small, which indicates that In-4*d* electronic states seem to be localized and show almost no dispersion.

Vibrational properties (phonons)

In order to understand the lattice dynamical stability and structural rigidity of all the six InN phases as considered, we have performed phonon-dispersion curve calculations. Figure 4a–f presents the phonon dispersion curves (PDC) along the high symmetric points in the Brillouin zone for all six phases. The dynamical matrix of the phonon dispersion is explicitly calculated on a $4 \times 4 \times 1$ and $4 \times 4 \times 4$ q-points meshes in monolayer and bulk, respectively, utilizing density functional perturbation theory (DFPT) by applying acoustic sum rule for $q \rightarrow 0$. It may be observed from the detailed analysis of the phonon spectra that unit cell of all the phases of InN (Fig. 3a–f) consists of 2, 4, 2, 2, 2 and 4 atoms, gives a total of six phonon branches for hexagonal, zinc blende, rock-salt and caesium chloride phases, whereas twelve branches for wurtzite and nickel arsenide phases, due to the number of atoms in their respective unit cells are one-third of the number of phonon branches. If there are n atoms per unit cell in

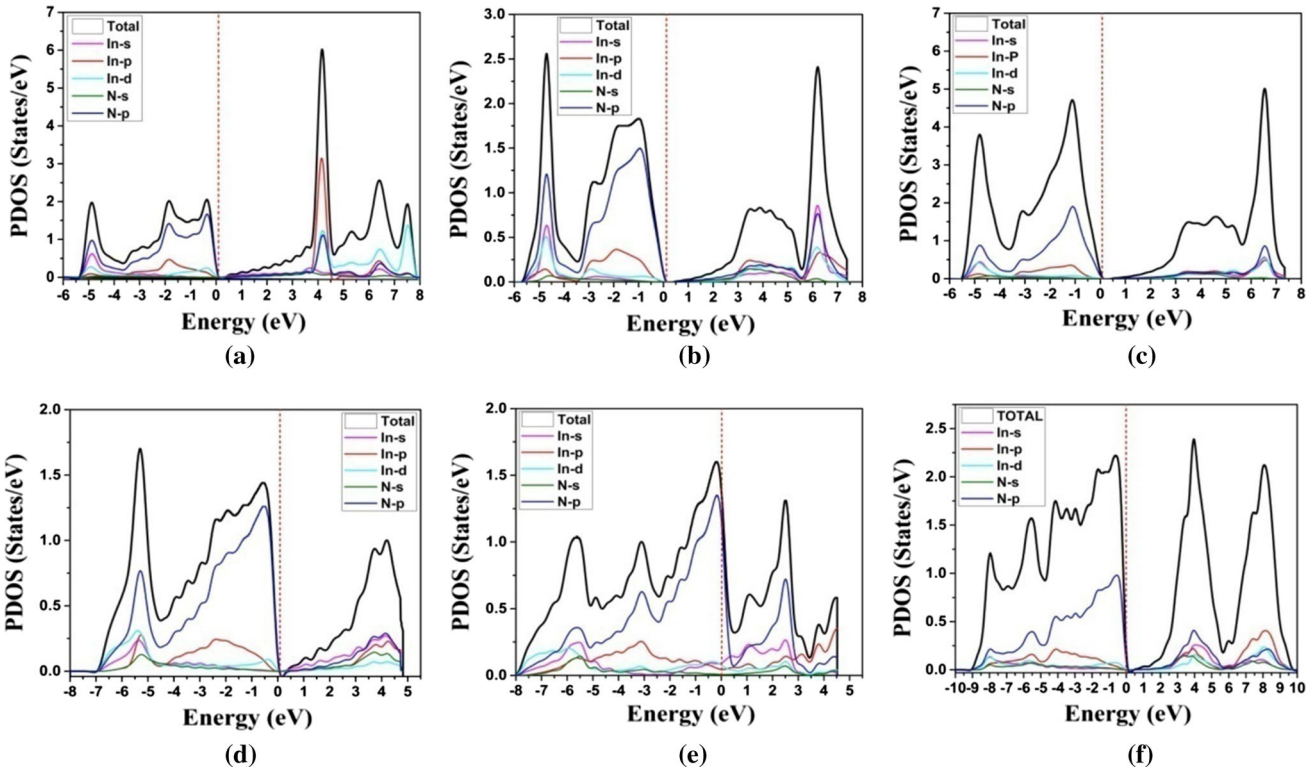

Figure 3 Total DOS and partial DOS for **a** monolayer hexagonal, **b** wurtzite, **c** zinc blende, **d** rock salt, **e** caesium chloride and **f** nickel arsenide phases of indium nitride.

the crystal structure, the total phonon branches would be 3n. Out of 3n branches, three would be considered as acoustic branch and the remaining (3n−3) are optical branch. Moreover, optical branch would be 3, 9, 3, 3, 3 and 9 in monolayer hexagonal, wurzite, zinc blende, rock salt, caesium chloride and nickel arsenide phases, respectively. It may be noted that among all six phases, degeneracy is mostly observed in wurtzite and nickel arsenide phases in out-of-plane acoustic (ZA) modes between Γ-M and Γ-K; moreover, in-plane transverse acoustic (TA) and out-of-plane optical (ZO) branches is slightly softer in the both cases from Γ–M and Γ–K points.

It may be noted that the frequencies of all phonon modes in PDC for the first four phases, viz. *h*-InN, *w*-InN, *zb*-InN and *rs*-InN, are found to be positive throughout the Brillouin zone and linear around Γ-point, indicating their dynamical stability. On the other hand, *cc*-InN and *na*-InN phases are found to have negative frequencies due to the shifting of acoustical branch in negative domain as a result of non-symmetric vibration of atoms at particular M and Γ points, respectively, in the Brillouin zone, indicating their dynamical instability. It may be of interest to note that although a large negative frequency (nearly 700 cm^{-1}) for caesium chloride phase shows significant instability of this phase, a small negative frequency range (less than 100 cm^{-1}) of nickel arsenide implies the viability of this newly explored phase of indium nitride at different ambient situations, e.g. in effect of external electric field, pressure and heat.

Although, among two of the dynamically instable phases caesium chloride have possible future aspects due to its small negative frequency and larger cohesive energy (9.75 eV), leaving the compound for a detail future investigation, we have further calculated various thermodynamic and thermoelectric properties, as well as electron density maps for the dynamically stable indium nitride phases, viz. *h*-InN, *w*-InN, *zb*-InN and *rs*-InN.

Thermodynamic properties

To gain insight into the thermodynamic behaviour of the four different dynamically stable phases for a large temperature range (up to 1000 K), we have calculated various the temperature-dependent

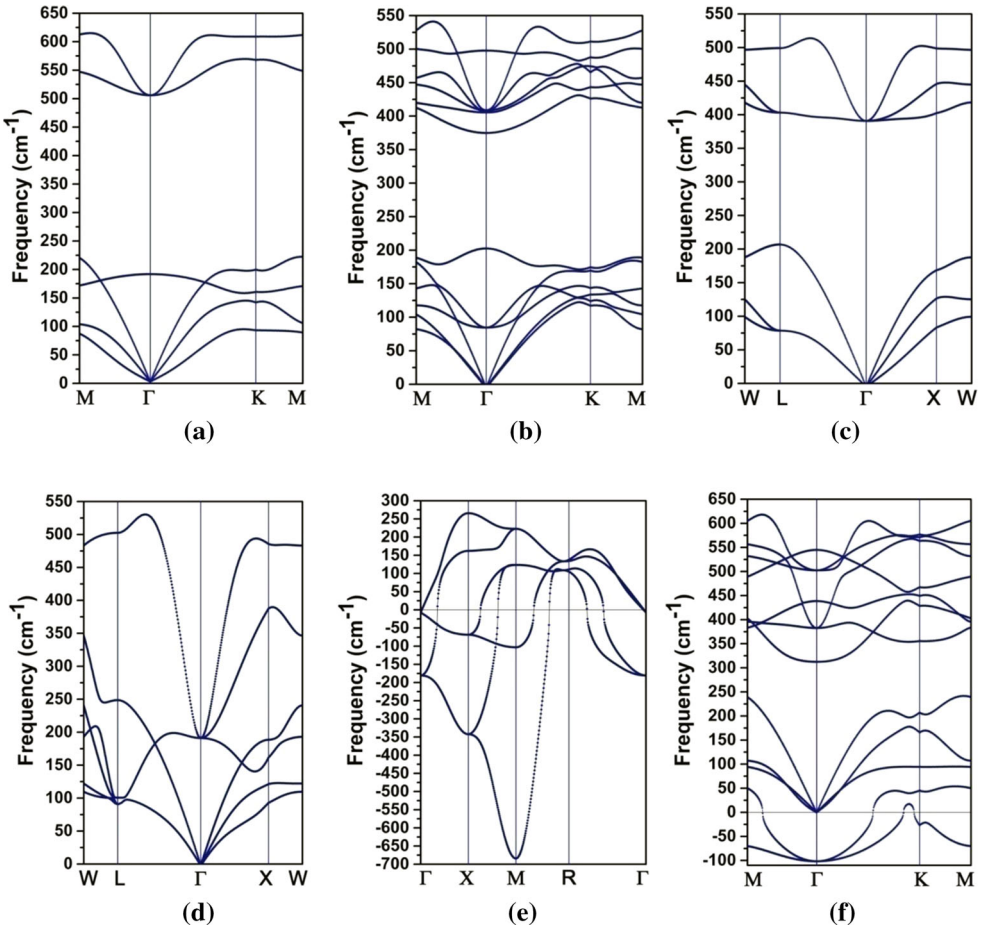

Figure 4 Phonon-dispersion curves of **a** monolayer hexagonal, **b** wurtzite, **c** zinc blende, **d** rock salt, **e** caesium chloride and **f** nickel arsenide phases of indium nitride.

thermodynamic functions, viz. specific heat at constant volume (C_v), entropy (S), internal energy (ΔU) and vibrational free energy (ΔF), as presented in Fig. 5a–d. It may be noted from Fig. 5a that the lattice specific heat (C_v) approaches the Dulong and Petit limit at high temperature for all hexagonal, wurtzite, zinc blende and rock salt InN phases, as expected. On the other hand, at very low temperatures, the specific heat varies third power of temperature (T^3) as per the Debye T^3 low and such a sharp rise of C_v due to long wavelength acoustical phonon. The lattice specific heat (C_v) is found to be maximum for hexagonal phase up to 150 K and lowest for wurtzite, after which it rises significantly for wurtzite phase and shows maximum towards Dulong Petit limit. The entropy (S), which is an extensive state function accounting the effects of irreversibility in thermodynamic states and a measure of disorder at molecular level, is an important quantity in thermodynamics and represented in Fig. 5b for all the stable phases of InN. As expected from the standard thermodynamic behaviour, the entropy continuously increases for all the phases with an increase in temperature. The wurtzite phase shows the lowest entropy up to 250 K, after which a sharp increase is noticed and shows maximum after 400 K compared to other phases. The hexagonal shows maximum entropy up to 400 K and shows larger entropy afterwards compared to zinc blende and rock salt phases. Entropy value for different phases up to 250 K follows the behaviour as hexagonal > rock salt > zinc blende > wurtzite, whereas after 400 K the relation follows as wurtzite > hexagonal > rock salt > zinc blende.

Figure 5c and d shows the variation of internal energy (ΔU) and vibrational free energy (ΔF) with increasing temperature for all the four phases. For all the phases, the internal energy increases with increasing temperature in which the wurtzite phase shows the maximum and rock salt as the lowest for the complete temperature range. The vibrational free energy (ΔF) which can be described as vibrational contribution of Helmholtz free energy for all four phases with respect to the increasing temperature is reported in Fig. 5d. A continuous decrease of ΔF

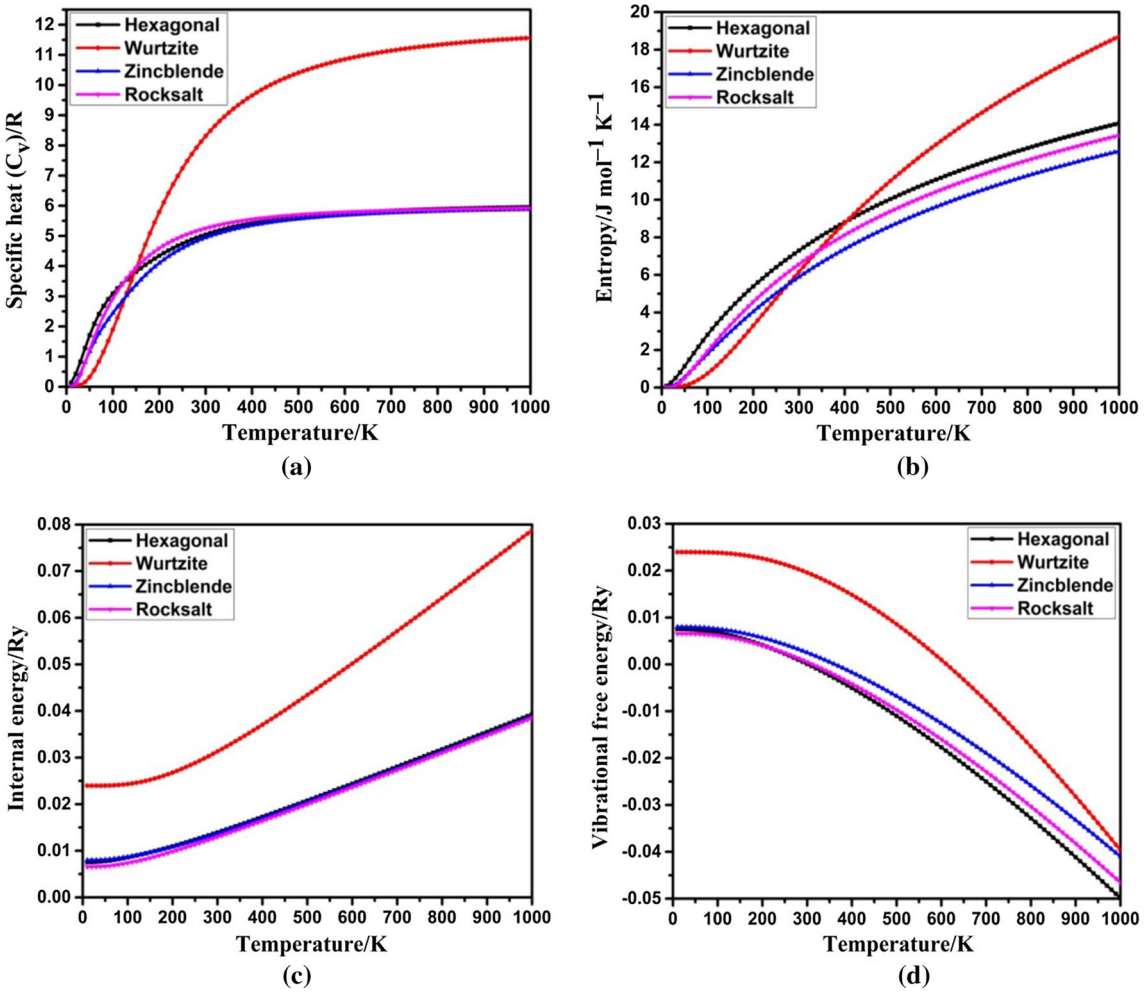

Figure 5 **a** Specific heat at constant volume **b** entropy **c** internal energy and **d** vibrational free energy of hexagonal, wurtzite, zinc blende and rock salt phases of indium nitride.

values is noticed for the phases with increasing temperature, in which the wurtzite phase shows the maximum value for the entire temperature range. It may be noted that the zero temperature vibrational free energy (ΔF_0) and internal energy (ΔU_0) are equal and is nonzero due to the zero point vibration. Overall, the wurtzite phase shows the highest specific heat, entropy, internal energy and vibrational free energy mostly with the increasing temperature compared to the other dynamically stable phases of indium nitride.

Thermoelectric properties

In order to understand the relative potential in thermoelectrical applications of the various stable phases of indium nitride, we have calculated both the electrical conductivity (σ) as well as thermal conductivity (κ) for large temperature range. Figure 6a and b represents the variation of electrical and thermal conductivities, respectively, of hexagonal, wurtzite, zinc blende and rock salt phases for a temperature range 200–700 K. It may be noted that the rock salt (*rs*-InN) phase shows very large electrical and thermal conductivities for the entire temperature range, which identifies it as a better InN phase for intermediate and high temperature thermoelectric applications compared to the other stable phases. The zinc blende shows more conductivities (σ and κ) compared to wurtzite and hexagonal, and overall the order of both types of conductivities are as follows: rock salt > zinc blende > wurtzite > hexagonal. In a recent study on the most stable wurtzite phase of indium nitride, Borges and Scolfaro [41] have

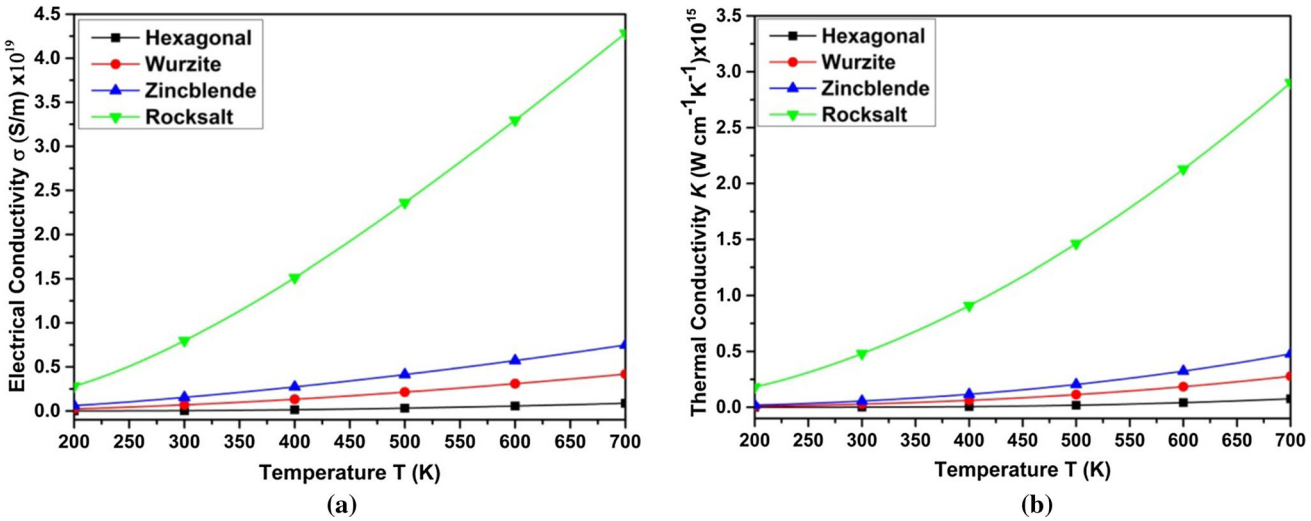

Figure 6 **a** Electrical and **b** thermal conductivities of hexagonal, wurtzite, zinc blende and rock salt phases of indium nitride.

reported *w*-InN phase has a potential for good thermoelectrical material. It is evident from the present work that rock salt followed by zinc blende phases may have better efficiency towards thermoelectrical applications compared to the most stable wurtzite phase.

Electron density contour

We have also predicted electron density contour for all the four stable indium nitride phase to understand the nature of bonding between indium and nitrogen in different phases. Figure 7 presents the two-dimensional charge density difference plots for hexagonal, wurtzite, zinc blende and rock salt phases of indium nitride. The contours are plotted along (110) for hexagonal (Fig. 7a) and wurtzite (Fig. 7b) phases, whereas (110) for zinc blende (Fig. 7c) and rock salt (Fig. 7d) phases the contours are plotted along (100) plane. The density values are plotted from -0.05 e/Å^3 to 0.05 e/Å^3 for monolayer hexagonal, wurtzite and zinc blende, and from -0.1 e/Å^3 to 0.1 e/Å^3 for rock salt phases. It can be noted that in all of the indium nitride phases, isolated electronic charge distributions on both the indium and nitrogen centres clearly indicating a strong ionic bonding nature between In and N. The positive

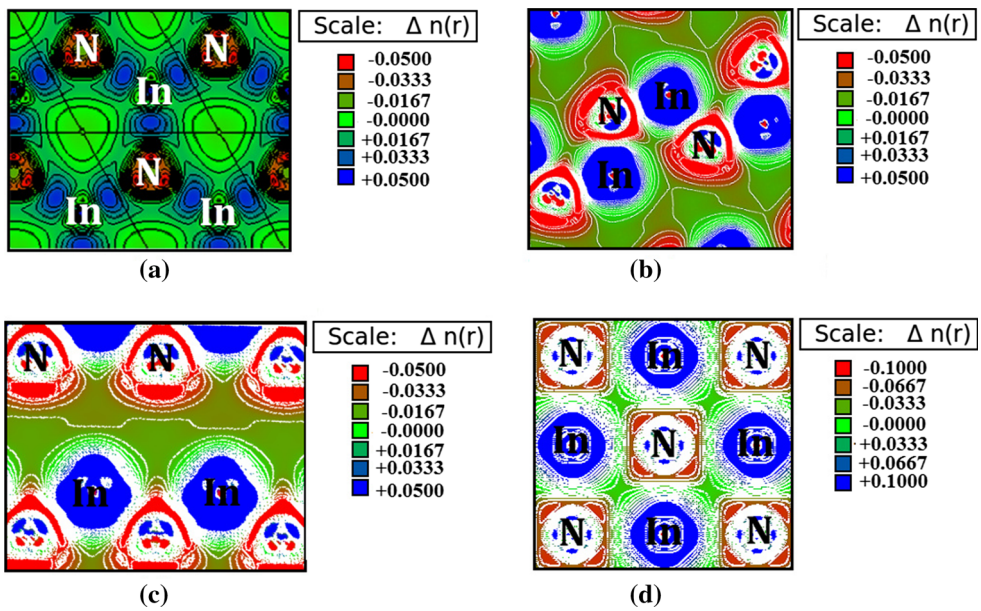

Figure 7 Contour plots of electron charge densities of **a** hexagonal, **b** wurtzite, **c** zinc blende and **d** rock salt phases of indium nitride.

electronic charge density on indium identifies them as cation centres, whereas nitrogen centres are understood as anionic centres due the accumulation of negative densities, which indicates a charge transfer from indium to nitrogen atom. Also, partly covalent bonding is also observed due to the hybridization between atom In-5*p* and N-2*p* states. A weak metallic bonding is also noticed in all the compounds due to the presence of density of states at or around Fermi level (E_F). In an overall observation, the bonding between indium and nitrogen atoms in all the four stable phases is mainly noticed to be ionic with a small partial contribution of covalent and metallic behaviour.

Conclusions

A detail and comparative study on the structure and bonding, electronic, thermodynamic and thermoelectric properties of six different phases of indium nitride is carried out. The monolayer hexagonal phase is found to be an indirect band gap (0.43 eV at Γ-K) semiconductor, whereas the other phase shows very close to zero band gap (small positive for wurtzite and zinc blende, and negative for rock salt and nickel arsenide) materials except for caesium chloride phase which appears to be metallic in nature. The PDOS analysis N (2*p*) states dominate at the Fermi level for all the six phases, whereas I (4*d*) states are seem to be localized and show hardly any dispersion. Among the six phases as considered, monolayer, wurtzite, zinc blende and rock salt phases found to be dynamically stable through phonon dispersion calculations. All the stable indium nitride phases found to obey the general thermodynamical behaviour, for example, specific heat (C_v) follows Debye T^3 low at very low temperature and at higher temperature it reaches the Dulong Petit's limit. The wurtzite phase is found to achieve the highest specific heat, entropy, internal energy and vibrational free energy on an average with the increasing temperature. The largest electrical and thermal conductivities of the rock salt followed by zinc blende phases imply there better usefulness towards thermoelectrical applications for a wide range of temperature, compared to the most stable wurtzite and the monolayer phases. It is evident from the present work that in spite of the small dynamical instability (negative frequency of less than 100 cm^{-1}) of the nickel arsenide phase, its significantly larger cohesive energy (9.75 eV, next to the wurtzite) and close to zero gap (slight band overlap at Γ point) open ups the scope for its further investigation at different ambient situations, e.g. in effect of external electric field, pressure and heat

Acknowledgements

DRR is thankful to the SERB, New Delhi, Govt. of India for financial support (Grant No. EMR/2016/005830). VK is thankful to the SERB, New Delhi, for his fellowship. DRR and VK are also thankful for the high-performance computing facility at CDAC, Pune and IUAC, New Delhi.

References

[1] Queren D, Avramescu A, Brüderl G, Breidenassel A, Schillgalies M, Lutgen S, Strau U (2009) 500 nm electrically driven InGaN based laser diodes. Appl Phys Lett 94:081119

[2] Zhang J, Kutlu S, Liu G, Tansu N (2011) High-temperature characteristics of Seebeck coefficients for AlInN alloys grown by metalorganic vapor phase epitaxy. J Appl Phys 110:043710

[3] Veal D, McConville CF, Schaff WJ (2009) Indium nitride and related alloys. Taylor & Francis, London

[4] Bierwagen O, Choi S, Speck JS (2011) Hall and seebeck profiling: determining surface, interface, and bulk electron transport properties in unintentionally doped InN. Phys Rev B 84:235302

[5] Sztein A, Ohta H, Bowers JE, DenBaars SP, Nakamura S (2011) High temperature thermoelectric properties of optimized InGaN. J Appl Phys 110:123709

[6] Wu J, Walukiewicz W, Yu KM, Ager Iii JW, Haller EE, Lu H, Nanishi Y (2002) Unusual properties of the fundamental band gap of InN. Appl Phys Lett 80:3967–3969

[7] Ghosh K, Rathore JS, Laha A (2017) Tuning the effective band gap and finding the optimal growth condition of InN thin films on GaN/sapphire substrates by plasma assisted molecular beam epitaxy technique. Superlattices Microstruct 101:405–414

[8] Ambacher O (1998) Growth and applications of group III-nitrides. J Phys Appl Phys 31:2653

[9] Elahi SM, Salehi H, Abolhassani MR, Farzan M (2016) A comparison of the structural, electronic, optical and elastic properties of wurtzite, zinc-blende and rock salt TlN: a DFT study. Acta Phys Pol A 130:758–768

[10] Dick KA, Caroff P, Bolinsson J, Messing ME, Johansson J, Deppert K, Samuelson L (2010) Control of III–V nanowire crystal structure by growth parameter tuning. Semicond Sci Technol 25:024009

[11] Peng F, Han Y, Fu H, Cheng X (2008) Phase transition, and elastic and thermodynamic properties of InN derived from first-principles and the quasi-harmonic Debye model (b). Physica status solidi 245:2743–2748

[12] Jung WS, Han OH, Chae SA (2007) Characterization of wurtzite indium nitride synthesized from indium oxide by In-115 MAS NMR spectroscopy. Mater Lett 61:3413–3415

[13] Miura A, Takei T, Kumada N (2012) Synthesis of wurtzite-type InN crystals by low-temperature nitridation of LiInO2 using NaNH2 flux. Cryst Growth Des 12:4545–4547

[14] Zhuang HL, Singh AK, Hennig RG (2013) Computational discovery of single-layer III–V materials. Phys Rev B 87:165415

[15] Goldhahn R, Winzer AT, Cimalla V, Ambacher O, Cobet C, Richter W, Schaff WJ (2004) Anisotropy of the dielectric function for wurtzite InN. Superlattices Microstruct 36:591–597

[16] Araujo RB, De Almeida JS, Ferreira Da Silva A (2013) Electronic properties of III-nitride semiconductors: a first-principles investigation using the Tran–Blaha modified Becke–Johnson potential. J Appl Phys 114:183702

[17] Zhang M, Zhang C, Liang D, Zhang R, Lu P, Wang S (2017) Structural and elastic properties of zinc-blende and wurtzite InN 1-x Bi x alloys. J Alloy Compd 708:323–327

[18] Kushwaha AK (2016) Lattice dynamical properties of group-III Nitrides AN (A = B, Al, Ga and In) in zinc-blende phase. Int J Thermophys 37:3–30

[19] Hohenberg P, Kohn W (1964) Inhomogeneous electron gas. Phys Rev 136:B864

[20] Kohn W, Sham LJ (1965) Self-consistent equations including exchange and correlation effects. Phys Rev 140:A1133

[21] Perdew JP, Burke K, Ernzerhof M (1996) Generalized gradient approximation made simple. Phys Rev Lett 77:3865

[22] Giannozzi P, Baroni S, Bonini N, Calandra M, Car R, Cavazzoni C, Dal Corso A (2009) QUANTUM ESPRESSO: a modular and open-source software project for quantum simulations of materials. J Phys Condens Matter 21:395502

[23] Ashcroft NW, Mermin ND (1976) Solid state physics. Cengage Learning. Inc., New York

[24] Kokalj A (2003) Computer graphics and graphical user interfaces as tools in simulations of matter at the atomic scale. Comput Mater Sci 28:155–168

[25] Yip S (ed) (2007) Handbook of materials modeling. Springer, Berlin

[26] Baroni S, De Gironcoli S, Dal Corso A, Giannozzi P (2001) Phonons and related crystal properties from density-functional perturbation theory. Rev Mod Phys 73:515–562

[27] Madsen GK, Singh DJ (2006) BoltzTraP. A code for calculating band-structure dependent quantities. Comput Phys Commun 175:67–71

[28] Scheidemantel TJ, Ambrosch-Draxl C, Thonhauser T, Badding JV, Sofo JO (2003) Transport coefficients from first-principles calculations. Phys Rev B 68:125210

[29] Jodin L, Tobola J, Pecheur P, Scherrer H, Kaprzyk S (2004) Effect of substitutions and defects in half-Heusler FeVSb studied by electron transport measurements and KKR-CPA electronic structure calculations. Phys Rev B 70:184207

[30] Stampfl C, Van de Walle CG (1999) Density-functional calculations for III–V nitrides using the local-density approximation and the generalized gradient approximation. Phys Rev B 59:5521

[31] Saoud FS, Plenet JC, Henini M (2012) Structural, electronic and vibrational properties of InN under high pressure. Physica B 407:1008–1013

[32] Mancera L, Rodríguez JA, Takeuchi N (2004) Theoretical study of the stability of wurtzite, zinc-blende, NaCl and CsCl phases in group IIIB and IIIA nitrides (b). Physica status solidi 241:2424–2428

[33] Furthmüller J, Hahn PH, Fuchs F, Bechstedt F (2005) Band structures and optical spectra of InN polymorphs: influence of quasiparticle and excitonic effects. Phys Rev B 72:205106

[34] Wang Y, Yin H, Cao R, Zahid F, Zhu Y, Liu L, Guo H (2013) Electronic structure of III–V zinc-blende semiconductors from first principles. Phys Rev B 87:235203

[35] Wyckoff RWG (1963) Fluorite structure, vol 1. Crystal structures. Interscience Publishers, New York, p 239

[36] Ueno M, Yoshida M, Onodera A, Shimomura O, Takemura K (1994) Stability of the wurtzite-type structure under high pressure: GaN and InN. Phys Rev B 49:14

[37] Duan M-Y, He L, Xu M et al (2010) Structural, electronic, and optical properties of wurtzite and rocksalt InN under pressure. Phys Rev B 81:033102

[38] Xia Q, Xia H, Ruoff AL (1994) New crystal structure of indium nitride: a pressure-induced rocksalt phase. Mod Phys Lett B 08:345–350

[39] Christensen NE, Gorczyca I (1994) Optical and structural properties of III–V nitrides under pressure. Phys Rev B 50:4397–4415

[40] Dufek P, Blaha P, Schwarz K (1994) Applications of Engel and Vosko's generalized gradient approximation in solids. Phys Rev B 50:7279

[41] Borges PD, Scolfaro L (2014) Electronic and thermoelectric properties of InN studied using ab initio density functional theory and Boltzmann transport calculations. J Appl Phys 116:223706

[42] Becke AD, Johnson ER (2006) A simple effective potential for exchange. Chicago

[43] Semchinova OK, Aderhold J, Graul J, Filimonov A, Neff H (2003) Photoluminescence, depth profile, and lattice instability of hexagonal InN films. Appl Phys Lett 83:5440–5442

[44] Jin H, Zhao GL, Bagayoko D (2007) Calculated optical properties of wurtzite InN. J Appl Phys 101:033123

[45] Perdew JP, Yang W, Burke K et al (2017) Understanding band gaps of solids in generalized Kohn–Sham theory. Proc Natl Acad Sci USA 114:2801–2806

[46] Pauling L (1960) The nature of the chemical bond and the structure of molecules and crystals: an introduction to modern structural chemistry, vol 18. Cornell University Press, Ithaca